

The continuous spectrum of bound states in expulsive potentials: self-trapping in the linear system

Hidetsugu Sakaguchi¹, Boris A. Malomed², Andreas C. Aristotelous³ and Efstathios G. Charalampidis⁴

¹*Interdisciplinary Graduate School of Engineering Sciences,
Kyushu University, Kasuga, Fukuoka 816-8580, Japan*

²*Department of Physical Electronics, School of Electrical Engineering,
Faculty of Engineering, and Center for Light-Matter Interaction,
Tel Aviv University, P.O. Box 39040 Tel Aviv, Israel*

³*Department of Mathematics, The University of Akron, OH 44325, USA and*

⁴*Department of Mathematics and Statistics and Computational Science Research Center,
San Diego State University, San Diego, CA 92182-7720, USA*

On the contrary to the common intuition, which suggests that a steep expulsive potential makes quantum states widely delocalized, we demonstrate that one- and two-dimensional (1D and 2D) Schrödinger equations, which include expulsive potentials that are *steeper than the quadratic* ones, give rise to *normalizable* eigenstates, which may be considered as a manifestation of *effective self-trapping in the linear system*. These states constitute full continuous spectra in both the 1D and 2D cases. In 1D, they are spatially even and odd eigenstates. The 2D states may carry any value of the vorticity (alias magnetic quantum number). Asymptotic expressions for wave functions of the 1D and 2D eigenstates, valid far from the center, are derived analytically, demonstrating excellent agreement with full numerical solutions. Special exact solutions for vortex states are obtained in the 2D case. These findings suggest an extension of the concept of bound states in the continuum, in quantum mechanics and paraxial photonics. Gross-Pitaevskii equations are briefly considered as the nonlinear extension of the 1D and 2D settings. In 1D, the cubic nonlinearity slightly deforms the eigenstates, maintaining their stability

Keywords: bound states in continuum; self-trapping; normalizability; asymptotic structure; cubic nonlinearity; parity-breaking instability; vorticity; angular momentum

I. INTRODUCTION AND METHODS

The separation of discrete and continuous spectra, which represent bound and delocalized states, respectively, is an underlying principle of the classical Sturm - Liouville theory [1–4] and quantum mechanics, whose mathematical framework is based on this theory [5, 6]. The fact that, in the paraxial approximation, the fundamental propagation equation for optical waves is tantamount to the quantum-mechanical Schrödinger equation makes the separation of discrete and continuous spectra an equally important tenet of optics [7–11]. This principle applies as well to other physical settings modeled by equations of the Schrödinger type [12, 13].

Nevertheless, there are well-known exceptions from the separation principle, in the form of *bound states embedded in the continuum* (often designated by the BIC acronym). The first example was discovered in 1929 by von Neumann and Wigner (vNW) [14], as a solution of the three-dimensional (3D) Schrödinger equation with the isotropic *expulsive* potential (written here in a scaled form),

$$U(r) = \frac{1}{r^2} - \frac{9}{2}r^4. \quad (1)$$

This potential supports a normalizable BIC stationary wave function,

$$\varphi_{\text{vNW}}(r) = \frac{1}{r^2} \sin(r^3) \quad (2)$$

(see Fig. 1), which corresponds to the zero energy eigenvalue. Later, schemes were designed for the realization of quantum-mechanical BIC states in semiconductor heterostructures [15, 16]. Then, much interest was drawn to BIC modes in various photonic setups, where they offer a considerable potential for applications [17–27].

In the framework of the mean-field approximation, the linear Schrödinger equation for a single atom is closely related to its nonlinear version in the form of the Gross-Pitaevskii equation (GPE), which includes the cubic term accounting for the averaged effect of inter-atomic collisions in the Bose-Einstein-condensate (BEC) phase of ultracold atomic gases [28]. In the optical realization, a model similar to GPE is based on the nonlinear Schrödinger equation (NLSE), which adds the Kerr self-focusing term to the paraxial propagation equation [7]. Under special conditions, NLSE-based optical models give rise to nonlinear states in the form of *embedded solitons*, which, similar to the BIC modes produced by the linear Schrödinger equation, may exist as peculiar localized states *embedded* in the continuous spectrum [29–34].

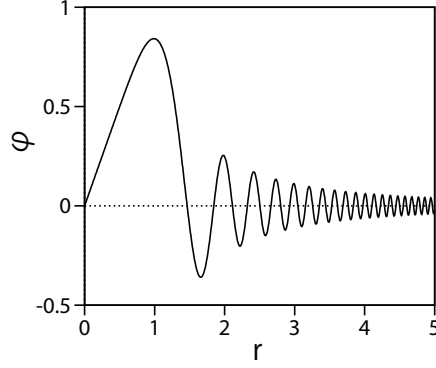


FIG. 1. The wave function $\varphi_{\text{vNW}}(r)$ of the von Neumann-Wigner BIC state.

Another counter-intuitive species of bound states is produced by a system of two linearly coupled 1D or 2D equations, each one being either a linear or nonlinear Schrödinger equation, with the usual trapping harmonic-oscillator (HO) potential in one equation, and the *expulsive* (anti-HO; alias inverted HO [35]) potential in the other [36]. The 2D linear system for wave functions u and v , written in the polar coordinates (r, θ) , is

$$i\frac{\partial u}{\partial t} + \frac{1}{2}\left(\frac{\partial^2}{\partial r^2} + \frac{1}{r}\frac{\partial}{\partial r} - \frac{1}{r^2}\frac{\partial^2}{\partial \theta^2}\right)u + \lambda v - \frac{1}{2}r^2u = -\omega u, \quad (3)$$

$$i\frac{\partial v}{\partial t} + \frac{1}{2}\left(\frac{\partial^2}{\partial r^2} + \frac{1}{r}\frac{\partial}{\partial r} - \frac{1}{r^2}\frac{\partial^2}{\partial \theta^2}\right)v + \lambda u + \frac{1}{2}\kappa r^2v = 0, \quad (4)$$

where λ is the coefficient of the linear coupling, $\kappa > 0$ is the relative strength of the anti-HO potential, while the HO strength in Eq. (3) is fixed to be 1 by scaling, and ω represents a possible eigenvalue mismatch between the coupled equations. It was found [36] that the system of Eqs. (3) and (4) admits bound-state solutions, in the form of

$$\{u, v\} = \exp(-iEt + iS\theta) \{U(r), V(r)\}, \quad (5)$$

with integer vorticity $S = 0, 1, 2, \dots$, real eigenvalue E (alias the chemical potential, in terms of BEC), which is a function of the system's parameters λ, ω, κ and vorticity S (as a special example, see Eq. (8) below), and stationary real wavefunctions which are localized as usual eigenstates of the 2D HO, i.e., $\{U(r), V(r)\} \sim r^S \exp(-r^2/2)$ at $r \rightarrow \infty$, despite the presence of the expulsive potential in Eq. (4). In particular, if the system's parameters are subject to constraint $\omega = (1/2)(5 + S - \lambda^2)$, the bound state is found as an exact solution,

$$u = U_0 [(\lambda^2 - 1 - S) + r^2] r^S \exp\left(-iE_{\text{exact}}t + iS\theta - \frac{r^2}{2}\right), \quad (6)$$

$$v = -2\lambda U_0 r^S \exp\left(-iE_{\text{exact}}t + iS\theta - \frac{r^2}{2}\right), \quad (7)$$

with the eigenvalue given by

$$E_{\text{exact}} = \frac{1}{2}(\lambda^2 + 1 + S), \quad (8)$$

where U_0 is an arbitrary amplitude. These strongly localized states, which exist with the single eigenvalue E , also represent BIC, as the same system gives rise to the continuous spectrum of weakly delocalized eigenstates, which are similar to the one given by Eq. (31) below.

The subject of the present work is to construct eigenstates of 1D and 2D linear and (in a brief form) nonlinear Schrödinger equations (alias GPEs) with expulsive potentials, taken as the quadratic anti-HO term ($\gamma = 1$ in Eq. (9)) or steeper ones ($\gamma > 1$; note that the vNW example (1) includes $\gamma = 2$). The respective 1D GPE for wave function $\psi(x, t)$ is introduced, in the scaled form, as

$$i\frac{\partial \psi}{\partial t} = -\frac{1}{2}\frac{\partial^2 \psi}{\partial x^2} - \frac{1}{2}x^{2\gamma}\psi + g|\psi|^{2\sigma}\psi, \quad (9)$$

where the coefficient in front of the potential term is fixed by means of scaling (cf. Eq. (3)), $g = -1, 0, +1$ correspond to the self-focusing, zero, or defocusing nonlinearity, and two physically relevant values, $\sigma = 1$ and 2 , represent, respectively, the cubic and quintic self-interaction. The cubic nonlinearity is the most generic one [7], while the quintic self-focusing, which can be implemented [37] and used [38] under well-controlled conditions in optics [37, 38], is interesting, as it gives rise to the 1D variety [39] of *Townes solitons* [40, 41]. Eigenstates produced by Eq. (9) with real eigenvalue E are looked for in the usual form, $\psi(x, t) = \exp(-iEt) \varphi(x)$, with stationary real eigenfunction $\varphi(x)$ satisfying the equation

$$E\varphi = -\frac{1}{2} \frac{d^2\varphi}{dx^2} - \frac{1}{2} x^{2\gamma} \varphi + g\varphi^{2\sigma+1}. \quad (10)$$

In the experiments with cold atoms, the expulsive anti-HO (quadratic) or steeper potential, in its 1D and 2D forms alike, can be readily imposed by a blue-detuned optical beam with the properly shaped transverse structure [43–45], or a red-tuned one with intrinsic vorticity [46–48]. The recently developed technique of programmable optical potentials [49–52] can also be used for this purpose.

One may intuitively expect that the strongly expulsive potential in Eq. (9) leads to strong delocalization of the respective eigenstates. Nevertheless, we demonstrate, analytically and numerically, that the intuition is misleading: the 1D and 2D linear Schrödinger equations with the anti-HO (quadratic) potential, $\gamma = 1$, give rise to weakly delocalized states, whose norm,

$$N_{1D} = \int_{-\infty}^{+\infty} \varphi^2(x) dx, \quad (11)$$

diverges logarithmically with the increase of the size of the solution domain (see Eq. (15) below), while all steeper expulsive potentials, corresponding to $\gamma > 1$, produce *effectively localized (self-trapped) bound states* with a convergent norm, which form a continuous spectrum ($-\infty < E < +\infty$). This situation seems unusual in quantum mechanics and BEC theory (as sort of a *quantum anomaly* [35, 53–56]) – in particular, because self-trapping is usually considered as the feature which may only be induced by the nonlinearity, while here it takes place in the linear setting.

While the most essential results are reported here in the framework of the 1D and 2D linear Schrödinger equations, some results for the 1D NLSE are reported, in a brief form, too. It is demonstrated that numerically found 1D bound states remain stable or develop parity-breaking instability, below or above a critical value of the norm N_{1D} , respectively, under the action of the cubic self-focusing term ($\sigma = 1$, $g = -1$) in Eq. (9) with the quartic expulsive potential ($\gamma = 2$).

Analytical and numerical results for the bound states in the 1D linear Schrödinger equation are reported in subsection 2A. This is followed, in subsection 2B, by a brief consideration of nonlinear bound states and their stability in the above-mentioned case, with parameters $\sigma = 1$, $g = -1$, and $\gamma = 2$ in Eq. (9). Findings for the 2D bound states, including vortex ones, which carry the angular momentum, are presented in subsection 2C (chiefly, for the linear Schrödinger equation). In particular, the consideration of the 2D linear Schrödinger equation with the expulsive potential produces *exact solutions* for the vortex states, under a special constraint imposed on the model's parameters. The paper is concluded by Section 3.

II. RESULTS

A. One-dimensional linear bound states

The starting point of the analysis is the linear version ($g = 0$) of the 1D stationary equation (10). While the equation is not analytically solvable, it is straightforward to construct its asymptotic solution, valid for sufficiently large values of $|x|$, in the form of a combination of rapidly oscillating cosines and sines, with amplitudes expanded in appropriate powers of $|x|^{-1}$. The analytical calculation is similar to the commonly known one which produces the asymptotic approximation for the Airy function [5]. Thus, the asymptotic approximation yields the result which is valid for $\gamma \neq 1$:

$$\varphi_{\text{asympt}}^{(1D)}(x; \gamma \neq 1; E) = \varphi_0 |x|^{-\gamma/2} \cos\left(\frac{|x|^{\gamma+1}}{\gamma+1} - \chi_0\right) + \frac{E\varphi_0}{\gamma-1} |x|^{-3\gamma/2+1} \sin\left(\frac{|x|^{\gamma+1}}{\gamma+1} - \chi_0\right), \quad (12)$$

where the amplitude φ_0 and phase shift χ_0 are arbitrary constants, in terms of the asymptotic solution. Note that setting $\gamma = 1/2$ in the first term in Eq. (12) reproduces the above-mentioned asymptotic approximation for the Airy

function. The approximation (12) retains the first two terms of the expansion, the third-order correction (TOC) being

$$\text{TOC} \left(\varphi_{\text{asympt}}^{(1\text{D})}(x); \gamma \neq 1 \right) = \frac{1}{8} \frac{\gamma(\gamma+2)}{\gamma+1} \varphi_0 |x|^{-3\gamma/2-1} \sin \left(\frac{|x|^{\gamma+1}}{\gamma+1} - \chi_0 \right). \quad (13)$$

An obvious property of the wave function (12) is the *convergence* of its integral norm, $N = \int_{-\infty}^{+\infty} \varphi^2(x) dx$ at $|x| \rightarrow \infty$, for $\gamma > 1$ and all eigenvalues $-\infty < E < +\infty$ (the full continuous spectrum). Thus, we arrive at a simple but counter-intuitive conclusion: any expulsive potential which is steeper than the quadratic (alias anti-HO) one, with $\gamma > 1$, produces *normalizable* bound states, which populate the full continuous spectrum. Qualitatively, this conclusion can be explained by noting that a classical counterpart of the quantum particle would be rolling down the steep potential hill with the rapidly growing acceleration, which gives rise to a strongly oscillating phase in the respective wave function, the latter feature leading to the *effective self-trapping* (localization/normalizability) of the eigenstate in the *linear system*, unlike the commonly known mechanism of self-trapping (creation of solitons) in various nonlinear models [7].

Note that all inflexion points ($d^2\varphi/dx^2 = 0$) of the stationary wave function produced by Eq. (10) with $g = 0$ and $E \geq 0$ coincide with zero-crossing ones, $\varphi(x) = 0$. In the case of $E < 0$, there are two additional inflexion points, *viz.*, $x = \pm (-2E)^{1/(2\gamma)}$.

The situation is different in the case of the anti-HO potential, with $\gamma = 1$ in Eq. (9). In this case, approximation (12) is replaced by the following one, which includes a logarithmic correction to the phase of the oscillatory wave function:

$$\varphi_{\text{asympt}}^{(1\text{D})}(x; \gamma = 1) = \varphi_0 |x|^{-1/2} \cos \left(\frac{x^2}{2} + E \ln \left(\frac{|x|}{l} \right) \right), \quad (14)$$

where l is a characteristic scale of the inner core of the wave function (an exact wave function of the 1D anti-HO potential can be formally expressed in terms of the special parabolic-cylinder function [35]). It follows from expression (14) that the respective normalization integral (11) slowly diverges,

$$N_{1\text{D}} \simeq \varphi_0^2 \ln(L/l), \quad (15)$$

$2L$ being the size of the integration domain.

The wave function of the 1D linear eigenstate, produced by a numerical solution of Eq. (10) with $g = 0$, $\gamma = 1$ (the anti-HO potential) and $E = 0$, and its comparison to the asymptotic approximation (12), are plotted in Fig. 2, with fitting constants $\chi_0 = \pi/8$ and $\varphi_0 = 1$ in Eq. (12) (in fact, φ_0 is an arbitrarily constant for the linear solution). The respective numerical solution of the second-order ordinary differential equation (10) was produced by means of the Runge-Kutta method, with the initial conditions

$$\varphi(x=0) = 1, \quad \frac{d\varphi}{dx}(x=0) = 0 \quad (16)$$

(which means that even solutions, with $\varphi(-x) = \varphi(x)$, were sought for). The same numerical method was used to obtain various eigenstates in what follows below. It is clearly observed that the analytical asymptotic approximation provides high accuracy, in comparison to its numerical counterpart.

In Fig. 2 it is not easy to display slowly decaying tails of the wave function, as the rapidly accelerating phase oscillations in Eq. (12) imply that the accurate numerical solution must take into regard spatial harmonics of very high orders. On the other hand, the asymptotic expression (12) yields the tails in the virtually exact analytical form.

A typical example of the *normalizable* (effectively self-trapped) 1D bound state for $\gamma = 2$ (the quartic expulsive potential), produced by the numerical solution of Eq. (10), and its comparison to the asymptotic approximation (12), is displayed in Fig. 3. In this case too, the asymptotic approximation demonstrates remarkably high accuracy.

For given E , the asymptotic expressions (12) and (13) may belong, at least, to two different global solutions (full eigenstates), *viz.*, the *fundamental* spatially even one, with $\varphi(-x) = \varphi(x)$ (alias the ground state, for given E), and the *dipole* spatially odd eigenstate, with $\varphi(-x) = -\varphi(x)$ (alias the first excited state). To illustrate this possibility for the same cases as considered above for the fundamental solutions, *viz.*, $\gamma = 1$ and $\gamma = 2$, the corresponding numerically found dipole eigenstates are plotted in Figs. 4(a) and (b), respectively. To this end, Eq. (10) was numerically solved again by means of the Runge-Kutta method, with the initial conditions

$$\varphi(x=0) = 0, \quad \frac{d\varphi}{dx}(x=0) = 1, \quad (17)$$

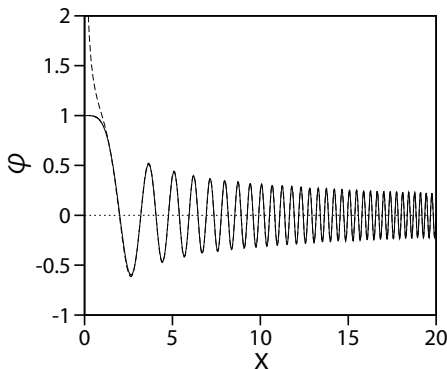


FIG. 2. The continuous curve: the numerically found spatially even solution of Eq. (10) with $g = 0$, $\gamma = 1$ (the quadratic expulsive potential) and $E = 0$. The dashed curve: the asymptotic approximation (12) for the same solution, with fitting constants $\chi_0 = \pi/8$ and $\varphi_0 = 1$.

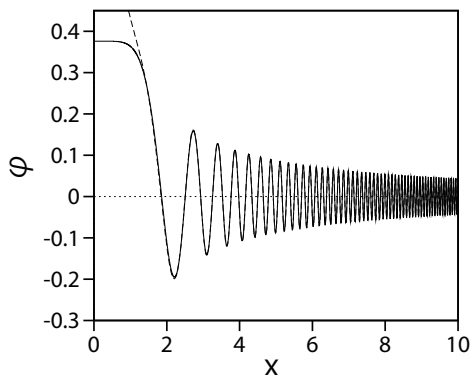


FIG. 3. The continuous curve: the numerically found spatially even solution of Eq. (10) with $g = 0$, $\gamma = 2$ (the quartic expulsive potential) and $E = 0$. The dashed curve: the asymptotic approximation (12) for the same case, with fitting constants $\chi_0 = \pi/6$ and $\varphi_0 = 0.44$.

cf. Eq. (16). It is plausible that Eq. (10) may produce additional spatially even and odd solutions, which correspond to higher-order excited states, in terms of quantum mechanics. This possibility will be considered elsewhere.

While the above examples display eigenstates found with the zero eigenvalue ($E = 0$), Fig. 5 presents a typical eigenstate for a very large negative eigenvalue, *viz.*, $E = -200$, in the case of $\gamma = 2$ (the quartic expulsive potential). It is seen that the large value of $-E$ suppresses the wave function in the core area of the eigenstate. At the inner edge of the core, the wave function quickly grows towards its largest value, attained at a point with $|x| = x_{\max}$, as $\varphi(x) \sim \exp(\sqrt{-2E}(x - x_{\max}))$, in agreement with Eq. (10). This is followed by the gradual decay of the rapidly oscillating tail, in agreement with Eq. (12). The dependence of x_{\max} on $|E|$ may be predicted, in a crude approximation, by equating the two respective large terms in Eq. (10), i.e., $-E\varphi \sim (1/2)x_{\max}^4\varphi$ (recall we here set $\gamma = 2$), which yields, in the logarithmic approximation,

$$\ln(x_{\max}) \simeq (1/4) \ln(-E). \quad (18)$$

This simple relation is compared to the numerical data in Fig. 6.

In the eigenstates corresponding to very large positive eigenvalues, the core area, $|x| \lesssim E^{1/4}$, is not (nearly) empty, unlike Fig. 6. Instead, it is filled by a nearly uniform standing wave, $\varphi(x) \approx \varphi(x=0) \cos(\sqrt{2E}x)$ (not shown here in detail).

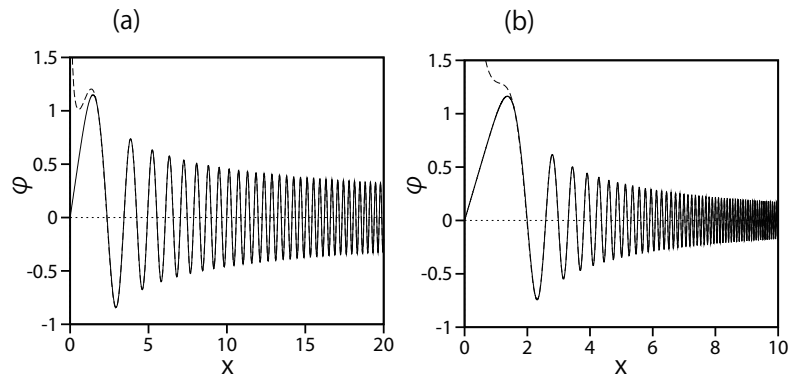


FIG. 4. In panels (a) and (b), the continuous curves represent numerically found spatially odd (dipole-mode) solutions of Eq. (10) with $g = 0$ and $E = 0$, for $\gamma = 1$ and 2 , respectively (cf. their spatially even (fundamental) counterparts displayed in Figs. 2 and 3, respectively). The dashed curves represent the corresponding asymptotic approximation (12) with fitting constants $\chi_0 = 3\pi/8$, $\varphi_0 = 1.45$ in (a), and $\chi_0 = \pi/3$, $\varphi_0 = 1.72$ in (b).

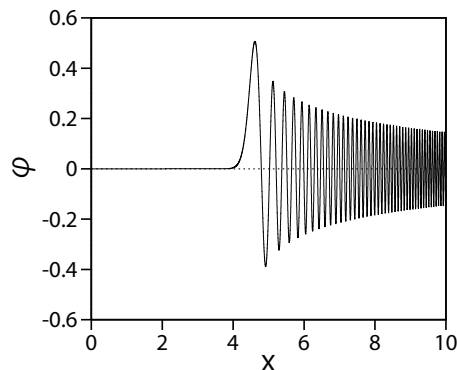


FIG. 5. The spatially even eigenstate produced by the numerical solution of Eq. (10) with $g = 0$, $\gamma = 2$, and $E = -200$.

B. Stable and unstable bound states in the 1D cubic nonlinear Schrödinger equation (NLSE) with the expulsive potential

While the stability of the existing eigenstates in the framework of the linear Schrödinger equation is obvious, it is a nontrivial problem in the case of the NLSE. The numerical solution of the stationary version of Eq. (9) with the cubic nonlinearity, i.e., $\sigma = 1$ and $g = \pm 1$, has demonstrated the existence of the corresponding bound states, with profiles somewhat deformed by the cubic term. Simulations of the perturbed evolution of the bound states have demonstrated that they remain stable in some parameter region, and become unstable in another, as briefly demonstrated below.

A typical example of the stable evolution of the bound state for $g = -1$ (the self-focusing cubic term), $\gamma = 2$ (the quartic expulsive potential), and $E = -0.9$ is presented in Fig. 7(a). In this case, the stationary even eigenstate (with $\varphi(-x) = \varphi(x)$) was obtained, as the solution of the corresponding ordinary differential equation (10), by dint of the Runge-Kutta method with the initial conditions $\varphi(x = 0) = 1.381$ and $d\varphi/dx(x = 0) = 0$, cf. Eq. (16). The stationary wave function vanishes at edges of the solution domain, $|x| = L = 4.8981$. The respective norm of the eigenstate, $\int_{-L}^{+L} \varphi^2(x) dx$ (cf. Eq. (11)) is

$$N_{1D} = 1.73. \quad (19)$$

To confirm the stability of this eigenstate, we have performed simulations of its perturbed evolution in the framework of the full equation (9), using the split-step Fourier method in the domain $|x| \leq L$, with zero boundary conditions, $\psi(x = \pm L) = 0$. The number of Fourier modes was 8192, and the marching timestep was $\Delta t = 10^{-5}$. As the local wavenumber of the oscillating tail increases with $|x|$, more Fourier modes are necessary for the simulations of a larger system. Here, we present the results of the simulations performed in the domain of size $2L = 9.7962$, which maintain

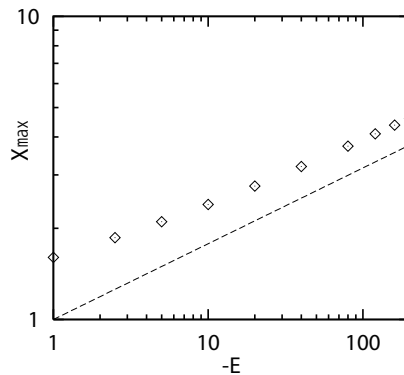


FIG. 6. The numerically found dependence of the coordinate x_{\max} , at which the wave function attains its maximum, on the eigenvalue $E < 0$, for $g = 0$ and $\gamma = 2$. The dependence is plotted on the log-log scale, with the straight dashed line representing the approximate relation (18).

sufficiently high numerical accuracy. As the initial condition, we took

$$\psi(x, t = 0) = \varphi(x) + 0.001 \sin(2\pi x/L), \quad (20)$$

where the second term introduces a small spatially odd perturbation, which breaks the parity of the nonlinear even eigenstate $\varphi(x)$. The aim was, in particular, to test the stability of the eigenstate against the spatial-symmetry-breaking perturbations. Eight snapshots of instantaneous profiles $|\psi(x, t)|$, produced by the simulations at $t = 0, 2, \dots, 14$, are plotted in Fig. 7(a). The presented results clearly confirm the stability of the nonlinear eigenstate.

A symmetry-breaking instability of the eigenstate occurs for larger absolute values of eigenvalue E . An example is presented in Fig. 7(b) for $g = -1$ and $E = -1.1$. The corresponding stationary eigenstate is produced by the numerical solution of Eq. (10) with the initial conditions $\varphi(x = 0) = 1.381$ and $d\varphi/dx(x = 0) = 0$, in the domain $0 < x < L = 4.9253$. The norm of the eigenstate is $N_{1D} = 3.07$, cf. the above value (19). Then, the perturbed evolution of the eigenstate was simulated with the input taken as per Eq. (20) (as above). Figure 7(b) shows snapshots of $|\psi(x, t)|$ at $t = 6, 8, \dots, 20$. It is seen that, unlike the stable evolution displayed in Fig. 7(a), the odd perturbation grows, so that the central-peak's position moves to the right and then returns to the origin, due to the interaction with the oscillatory tail.

The motion of the center of mass of the solutions,

$$\langle x \rangle = \frac{1}{N_{1D}} \int_{-L}^{+L} x |\psi(x)|^2 dx, \quad (21)$$

is plotted in Fig. 7(c) for the above-mentioned perturbed eigenstates with $E = -0.9$ (the dotted red line), $E = -1.1$ (the dashed blue line), and also for the intermediate case, with $E = -1.0$, with $L = 4.9116$ and $N_{1D} = 2.86$ (the solid green line). It is concluded that the parity-breaking instability of the spatially even nonlinear eigenstates occurs at $E \approx -1$, a natural conclusion being that the self-focusing nonlinearity leads to the destabilization of the bound states above a critical value of the norm. In particular, the dashed blue trajectory in Fig. 7(c) demonstrates that cycle of the instability development, which is displayed in Fig. 7(b), repeats with approximate periodicity. Detailed studies of the stability of the nonlinear eigenstates, and production of the respective stability charts for the systems with of the cubic and quintic nonlinear terms, will be a subject of another work.

The 1D spatially odd (dipole) eigenstates are also weakly deformed by the cubic nonlinearity, and may remain stable, depending on the parameters. An example is displayed in Fig. 8 for $\gamma = 2$, $\sigma = 1$, $g = +1$ (the self-defocusing cubic term) and $E = 0$, i.e., the same parameters as those (except for $g = 0$) of the dipole-mode eigenstate shown in Fig. 4(b), which was produced by the linear version of Eq. (10). Note that both eigenstates are very well approximated by the asymptotic expression (12) with appropriate values of the fitting constants, *viz.*, $\chi_0 = \pi/3$ for $g = 0$ and $\chi_0 = 5\pi/12$ for $g = +1$.

C. Two-dimensional bound states

The natural 2D version of Eq. (9) can also be realized experimentally as the GPE for ultracold atoms, under the action of the isotropic expulsive optical potential, induced by the blue-detuned laser beam, or the red-detuned one

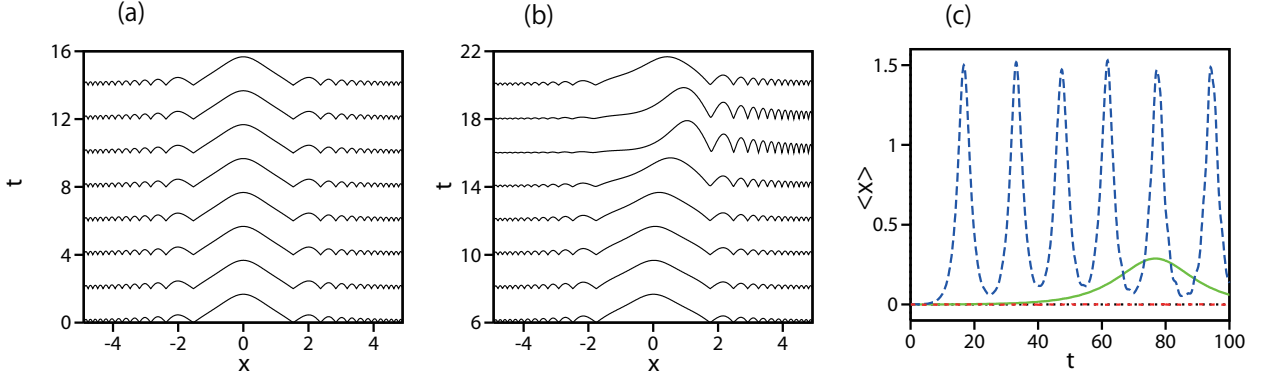


FIG. 7. (a) The stable evolution of the spatially even eigenstate obtained as the numerical solution of Eq. (10) with $\gamma = 2$, $g = -1$, $\sigma = 1$ (the cubic self-focusing nonlinearity), eigenvalue $E = -0.9$, and norm $N_{1D} = 1.73$. Eight snapshots of $|\psi(x, t)|$ at $t = 0, 2, \dots, 14$ are plotted. (b) Snapshots of $|\psi(x, t)|$ at $t = 6, 8, \dots, 20$ illustrate the onset of the spontaneous parity-breaking instability of the even eigenstate with $E = -1.1$ and $N_{1D} = 3.07$. (c) The center-of-mass coordinate (21) as a function of time for the perturbed evolution of the eigenstates with $E = -0.9$ (the dotted red line), $E = -1$ (the solid green line), and $E = -1.1$ (the dashed blue line).

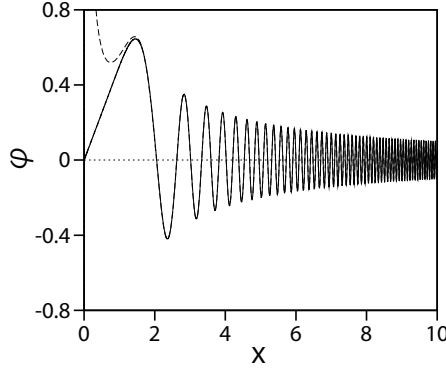


FIG. 8. The stable spatially odd eigenstate produced by the numerical solution of Eq. (10) with $g = +1$, $E = 0$, and $\gamma = 2$, cf. its counterpart plotted in Fig. 4(b) produced for the same parameters by the linearized equation (with $g = 0$). The norm of the eigenstate is $N = 1.23$. The dashed curve represents the corresponding asymptotic approximation (12) with fitting constants $\chi_0 = 5\pi/12$ and $\varphi_0 = 0.995$.

with intrinsic vorticity. In terms of the polar coordinates (r, θ) , the 2D GPE is written as

$$i \frac{\partial \psi}{\partial t} = -\frac{1}{2} \left(\frac{\partial^2 \psi}{\partial r^2} + \frac{1}{r} \frac{\partial \psi}{\partial r} + \frac{1}{r^2} \frac{\partial^2 \psi}{\partial \theta^2} \right) - \frac{1}{2} r^{2\gamma} \psi + g |\psi|^2 \psi, \quad (22)$$

with $\gamma \geq 1$ (here, only the cubic nonlinear term is considered, if any). The stationary version of Eq. (22) with integer vorticity S (alias magnetic quantum number) and eigenvalue E (the chemical potential, in terms of the BEC), is produced by the substitution

$$\psi = \exp(-iEt + iS\theta) \varphi(r), \quad (23)$$

where real function $\varphi(r)$ obeys the equation

$$E\varphi = -\frac{1}{2} \left(\frac{d^2 \varphi}{dr^2} + \frac{1}{r} \frac{d\varphi}{dr} - \frac{S^2}{r^2} \varphi \right) - \frac{1}{2} r^{2\gamma} \varphi + g\varphi^3. \quad (24)$$

Similar to Eq. (12) in the 1D case, it is straightforward to construct the asymptotic form of the tail of the solution to Eq. (24) at $r \rightarrow \infty$, in the case of $\gamma \neq 1$. The first two terms of the asymptotic expansion are

$$\varphi_{\text{asympt}}^{(2D)}(r) = \varphi_0 r^{-(\gamma+1)/2} \cos\left(\frac{r^{\gamma+1}}{\gamma+1} - \chi_0\right) + \frac{E\varphi_0}{\gamma-1} r^{-(3\gamma-1)/2} \sin\left(\frac{r^{\gamma+1}}{\gamma+1} - \chi_0\right), \quad (25)$$

and the TOC term is

$$\text{TOC} \left(\varphi_{\text{asympt}}^{(2D)}(x) \right) = \varphi_0 \frac{(\gamma + 1)^2 - 4S^2}{2(2\gamma + 1)} r^{-3(\gamma+1)/2} \sin \left(\frac{r^{\gamma+1}}{\gamma + 1} - \chi_0 \right), \quad (26)$$

cf. its 1D counterpart (13). As above, φ_0 and χ_0 are indefinite constants, in the framework of the asymptotic expansion at $r \rightarrow \infty$. Note that only the higher-order correction to the asymptotic expansion, given by Eq. (26), includes the vorticity.

As seen from expression (25), the 2D norm of these eigenstates, $N_{2D} = 2\pi \int_0^\infty \varphi^2(r) r dr$, converges under precisely the same condition as in 1D, *viz.*, $\gamma > 1$, i.e., if the 2D expulsive potential is *steeper* than the isotropic anti-HO (quartic) potential. A qualitative explanation for this counter-intuitive conclusion is the same as in the 1D setting: under the action of the expulsive potential, a classical particle would be rolling down the steep potential hill (along a spiral trajectory, if the particle carries the angular momentum, corresponding to $S \geq 1$ in expression (23)), with rapid acceleration. In terms of the particle's quantum counterpart, the acceleration gives rise to the strongly oscillating phase of the wave function, thus leading to the effective *linear self-trapping* (localization) of the eigenstate, with the normalizable wavefunction.

Similar to the 1D case, for the 2D Schrödinger equation (22) with $\gamma = 1$ (the anti-HO expulsive potential), the asymptotic expression (25) takes a different form, with the logarithmic correction to the phase of the rapid oscillations:

$$\varphi_{\text{asympt}}^{(2D)}(r; \gamma = 1) = \varphi_0 r^{-1} \cos \left(\frac{r^2}{2} + E \ln \left(\frac{r}{l} \right) \right), \quad (27)$$

where l is the radius of the inner core, cf. Eq. (14). Also similar to its 1D counterpart, in the case of $\gamma = 1$ the norm of the 2D eigenstate is weakly divergent, $N_{2D} \simeq \pi \varphi_0^2 \ln(L/l)$ (cf. Eq. (15)), where L is the radius of the integration domain.

An additional analytical result, which is not available in the 1D case, is the existence of particular *exact solutions* to the linear version Eq. (24), with $g = 0$ and $E = 0$, if the power factor γ of the expulsive potential in Eq. (22) is selected, for given integer vorticity $S \geq 1$, as

$$\gamma(S) = 2S - 1. \quad (28)$$

In this case, the exact wave function is

$$\varphi_{\text{exact}}(r; S) = \frac{\varphi_0}{r^S} \sin \left(\frac{r^{2S}}{2S} \right), \quad (29)$$

where φ_0 is an arbitrary amplitude. For all values $S \geq 2$, the norm of the exact wave function (29) converges, yielding

$$(N_{2D})_{\text{exact}} = 2\pi \int_0^\infty \varphi_{\text{exact}}^2(r; S) r dr = \varphi_0^2 \frac{\pi \Gamma(1/S)}{2S^{1-(1/S)}(S-1)} \cos \left(\frac{\pi}{2} \left(1 - \frac{1}{S} \right) \right). \quad (30)$$

where $\Gamma(1/S)$ is the Gamma-function. In agreement with the above conclusions, the norm diverges for $\gamma = 1$, i.e., $S = 1$, see Eq. (28), the respective exact solution (29) taking the form of

$$\varphi_{\text{exact}}(r; S = 1) = \frac{\varphi_0}{r} \sin \left(\frac{r^2}{2} \right). \quad (31)$$

This analytical solution and the corresponding numerical solution of Eq. (24), with $\varphi_0 = 0.409$, are plotted by the solid and dashed lines, respectively, in Fig. 9(a), where they completely overlap (actually, the coincidence with the exact analytical solution corroborates the accuracy of the numerical solution). The 2D structure of this vortex eigenstate is illustrated by means of the color plot in Fig. 9(b).

Lastly, if the cubic term is retained in Eq. (24) with $\gamma = 1$ (the anti-HO expulsive potential), one can construct an approximate solution for $E = 0$ and $S \neq 1$, neglecting the third harmonic in the elementary formula $\sin^3 \Phi = (3/4) \sin \Phi - (1/4) \sin(3\Phi)$. The respective approximate solution is given by Eq. (31) (even if S is not 1), in which the amplitude is determined by the balance of the linear and nonlinear terms in Eq. (24):

$$\varphi_0^2 = 2(3g)^{-1} (1 - S^2). \quad (32)$$

Thus, the approximate solution (31) of Eq. (24) with the self-defocusing or focusing nonlinearity, i.e., $g = +1$ or $g = -1$, exists, yielding $\varphi_0^2 > 0$ as per Eq. (32), for $S = 0$ or $S \geq 2$, respectively.

In the case of $g = -1$ (self-focusing), it is necessary to test the stability of the nonlinear vortex solutions against spontaneous splitting, cf. Refs. [57–59]. These results will be reported elsewhere.

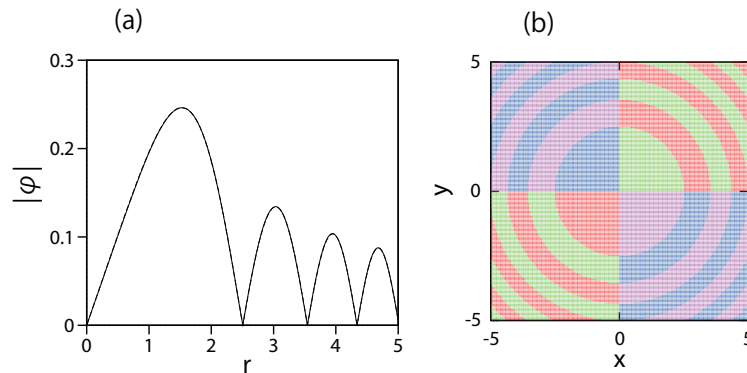


FIG. 9. (a) The absolute value $|\varphi(r)|$ of the exact solution (31) of Eq. (24) with $\varphi_0 = 0.409$ for $\gamma = 1$, $g = 0$, $S = 1$, and $E = 0$. (b) The color snapshot of this 2D vortex state at $t = 0$, $\psi(r, \theta) \equiv \varphi(r)e^{i\theta}$: $\text{Re}\psi > 0$ and $\text{Im}\psi > 0$ in the green region, $\text{Re}\psi < 0$ and $\text{Im}\psi > 0$ in the blue region, $\text{Re}\psi < 0$ and $\text{Im}\psi < 0$ in the red region, $\text{Re}\psi > 0$ and $\text{Im}\psi < 0$ in the purple one.

III. CONCLUSIONS

Our analysis demonstrates that, on the contrary to the intuitive expectation, the 1D and 2D Schrödinger equations with the expulsive potential which is steeper than the quadratic (anti-HO) one, generates a full continuous spectrum of the *normalizable* bound states, which may be considered as a manifestation of the *effective self-trapping in the linear system*. In 1D, these bound states may be the fundamental and dipole ones (spatially even and odd modes, respectively; plausibly, higher-order excited states exist too, which is a subject for additional analysis). The 2D bound states may carry any integer vorticity (angular momentum). Universal asymptotic expressions for the 1D and 2D states, valid at $|x| \rightarrow \infty$ and $r \rightarrow \infty$, respectively, are found, providing an extremely accurate approximation to the numerically found wave functions. In addition, in the 2D case special vorticity-carrying solutions are found in the exact form. These results essentially extend the concept of BIC (bound states in the continuum), which has recently drawn much interest in the context of photonics, where the paraxial-propagation models amount to the same Schrödinger equations as in quantum mechanics. In the case of the anti-HO (quadratic) shape of the expulsive potential, the normalization integrals for the bound states are weakly divergent, in 1D and 2D settings alike. The nonlinear version of the 1D and 2D models, in the form of the respective GPEs (Gross-Pitaevskii equations), are briefly considered too. In 1D, the cubic self-focusing or defocusing nonlinearity slightly deforms the linear solutions. A parity-breaking instability occurs in the case of the self-focusing nonlinearity if the norm of the spatially even eigenstate exceeds a critical value. A detailed analysis of the nonlinear models will be reported elsewhere. In particular, a challenging issue is the (in)stability of 2D nonlinear vortex eigenstates against splitting by the azimuthal modulational instability in the case of the self-focusing cubic nonlinearity. In parallel, it is relevant to perform the spectral stability analysis of the nonlinear eigenstates, in the framework of the Bogoliubov-de Gennes equations for small perturbations [60, 61]. As concerns the development of the numerical analysis of the 1D and 2D eigenstates reported in this work, a challenging issue is the need of using a large number of grid points for capturing rapid oscillations of the decaying tails. A potential way to improve this aspect of the 2D solutions may be the use of the mesh adaptation [62], that should help resolving the oscillations very accurately with less computational cost. These studies are currently underway and will be reported elsewhere.

IV. ACKNOWLEDGMENTS

We thank P. G. Kevrekidis and D. H. J. O'Dell for helpful discussions.

V. FUNDING

E.G.C. acknowledges support from the San Diego State University, Department of Mathematics and Statistics startup fund.

VI. AUTHOR CONTRIBUTIONS

Software development and numerical calculations: H.S., A.C.A., and E.C. Analytical considerations: B.A.M. and H.S. Analysis of the results: all authors. Drafting the manuscript: B.A.M. H.S, and A.C.A.

VII. CONFLICT OF INTERESTS

Authors declare no conflict of interests

VIII. DATA AVAILABILITY STATEMENT

The data supporting the findings of this publication can be made available upon request.

-
- [1] Zettl A., *Sturm–Liouville Theory* (AMS, Providence, 2005).
- [2] Lin J. S. and Zhang H., Mathematical theory for topological photonic materials in one dimension, *J. Phys. A: Math. Gen.* **55**, 495203 (2022); DOI 10.1088/1751-8121/aca9a5.
- [3] Chu J. F., Meng G., and Zhang Z., Minimizations of positive periodic and Dirichlet eigenvalues for general indefinite Sturm-Liouville problems, *Advances in Mathematics* **432**, 109272 (2023), <https://doi.org/10.1016/j.aim.2023.109272>.
- [4] Kravchenko V. V., Spectrum completion and inverse Sturm-Liouville problems, *Mathematical Methods in the Applied Sciences* **46**, 5821-5835 (2023), <https://doi.org/10.1002/mma.8869>.
- [5] Landau L. D. and Lifshitz E. M., *Quantum Mechanics* (Nauka publishers, Moscow, 1974).
- [6] Ballentine L. E., *Quantum Mechanics* (World Scientific, Singapore, 2000).
- [7] Kivshar Y. S. and Agrawal G. P., *Optical Solitons: From Fibers to Photonic Crystals* (Academic Press, San Diego, 2003).
- [8] Chen Z., Segev M., and Christodoulides D. N., Optical spatial solitons: historical overview and recent advances, *Rep. Prog. Phys.* **75**, 086401 (2012), doi:10.1088/0034-4885/75/8/086401.
- [9] Gillen G. D., Gillen K., and Guha S., *Light Propagation in Linear Optical Media* (Taylor & Francis, Boca Raton, 2014).
- [10] Briggs J. S., The propagation of Hermite-Gauss wave packets in optics and quantum mechanics, *Natural Sciences* **4**, e202300912 (2024), DOI: 10.1002/ntls.20230012.
- [11] Wang K. L. and Wei C. F., Novel optical soliton solutions to nonlinear paraxial wave model, *Mod. Phys. Lett. B* **39**, 2450469 (2025), <https://doi.org/10.1142/S0217984924504694>.
- [12] Yang J., *Nonlinear Waves in Integrable and Nonintegrable Systems* (SIAM, Philadelphia, 2010).
- [13] Carretero-González, R., Frantzeskakis D. J., and Kevrekidis, P. G., *Nonlinear Waves & Hamiltonian Systems: From One To Many Degrees of Freedom, From Discrete To Continuum* (Oxford University Press, Oxford, 2024).
- [14] von Neumann J. and Wigner E., Über merkwürdige diskrete Eigenwerte, *Phys. Z.* **30**, 465-467 (1929).
- [15] Stillinger F. H., Potentials supporting positive-energy eigenstates and their application to semiconductor heterostructures, *Physica B* **85**, 270–276 (1976); [https://doi.org/10.1016/0378-4363\(76\)90021-8](https://doi.org/10.1016/0378-4363(76)90021-8).
- [16] Friedrich H. and Wintgen, D., Interfering resonances and bound states in the continuum, *Phys. Rev. A* **32**, 3231–3242 (1985); DOI: <https://doi.org/10.1103/PhysRevA.32.3231>.
- [17] Marinica D. C., Borisov A. G., and Shabanov S. V., Bound states in the continuum in photonics, *Phys. Rev. Lett.* **100**, 183902 (2008); DOI: <https://doi.org/10.1103/PhysRevLett.100.183902>.
- [18] C. W. Hsu, Zhen B., Stone A. D., Joannopoulos J. D., and Soljačić M., Bound states in the continuum, *Nature Rev. Mat.* **9**, 16048 (2016); <https://doi.org/10.1103/PhysRevLett.100.183902>.
- [19] Kodigala A., Lepetit T., Gu Q., Bahari B., Fainman Y., and Kanté B., Lasing action from photonic bound states in continuum, *Nature* **541**, 196-199 (2017); <https://doi.org/10.1038/nature20799>.
- [20] Shi T., Deng Z. L., Geng G., Zeng X., Zeng Y., Hu G., Overvig A., Li J., Qiu C.-W., Alù A., Kivshar Y. S., and Li X., Planar chiral metasurfaces with maximal and tunable chiroptical response driven by bound states in the continuum, *Nature Communications* **13**, 4111 (2022), <https://doi.org/10.1038/s41467-022-31877-1>.
- [21] Santiago-Cruz T., Sylvain D. Gennaro S. D., Mitrofanov O., Addamane S., Reno J., Brener I., and V. Chekhova M. V., Resonant metasurfaces for generating complex quantum states, *Science* **377**, 991-995 (2022); DOI: 10.1126/science.abq8684.
- [22] Chen Y., Deng H., Sha X., Chen W., Wang R., Chen Y.-H., Wu D., Chu J., Kivshar Y. S., Xiao S., and Qiu C.-W., Observation of intrinsic chiral bound states in the continuum. *Nature* **613**, 474-479 (2023); <https://doi.org/10.1038/s41586-022-05467-6>.
- [23] Kang M., Liu T., Chan C. T., and Xiao, M., Applications of bound states in the continuum in photonics, *Nature Rev. Phys.* **5**, 659-678 (2023); <https://doi.org/10.1038/s42254-023-00642-8>.
- [24] Huang L, Xu L. Powell D. A., Padilla W. J., and Miroshnichenko A. E., Resonant leaky modes in all-dielectric metasystems: Fundamentals and applications, *Phys. Rep.* 1008, 1-66 (2023), <https://doi.org/10.1016/j.physrep.2023.01.001>.

- [25] Liu B., Peng Y., Jin Z., Wu X., Gu H., Wei. D., Zhu Y., and Zhuang S., Terahertz ultrasensitive biosensor based on wide-area and intense light-matter interaction supported by QBIC, *Chemical Engineering Journal* **462**, 142347 (2023), <https://doi.org/10.1016/j.cej.2023.142347>.
- [26] Wu X., Zhang S., Song J., Deng X., Du W., Zeng X., Zhang Y., Zhang Z., Chen Y., Wang Y., Jiang C., Zhong Y., Wu B., Zhu Z., Liang Y., Zhang Q., Xiong Q., and Liu X. Exciton polariton condensation from bound states in the continuum at room temperature. *Nature Communications* **15**, 3345 (2024); DOI:10.1038/s41467-024-47669-8.
- [27] Zhao, W. K., Wang S. Y., Jing Y. H., Ge H., Wang Q., Zeng Y. Q., Jia B. W., and Xu N. Giant structurally modulated intrinsic chirality of quasi-bound states in continuum. *Optics Letters* **50**, 1649-1652 (2025); <https://doi.org/10.1364/OL.549705>.
- [28] Pitaevskii L. P. and Stringari S., *Bose-Einstein Condensation* (Oxford University Press, Oxford, 2003).
- [29] Champneys A. R., Malomed B. A., Yang J., and Kaup D. J., “Embedded solitons” : solitary waves in resonance with the linear spectrum, *Physica D* **152-153**, 340-354 (2001); [https://doi.org/10.1016/S0167-2789\(01\)00178-6](https://doi.org/10.1016/S0167-2789(01)00178-6).
- [30] Doak A., Barros R., and Milewski P. A., Large mode-2 internal solitary waves in three-layer flows, *J. Fluid Mech.* **953**, A42 (2022); doi:10.1017/jfm.2022.974
- [31] Kudryashov N. A., Mathematical model with unrestricted dispersion and polynomial nonlinearity, *Appl. Math. Lett.* **138**, 108519 (2023), <https://doi.org/10.1016/j.aml.2022.108519>.
- [32] Li Z. and Peng C., Dynamics and Embedded Solitons of Stochastic Quadratic and Cubic Nonlinear Susceptibilities with Multiplicative White Noise in the Itô Sense, *Mathematics* **11**, 3185 (2023), <https://doi.org/10.3390/math11143185>.
- [33] Rizvi S. T. R., Seadawy A. R., Nimra, Ali K., and Aziz N., Variety of optical soliton solutions via sub-ODE approach to embedded soliton generating model in quadratic nonlinear media, *Int. J. Mod. Phys. B* **37**, 2350137 (2023); <https://doi.org.rproxy.tau.ac.il/10.1142/S0217979223501370>.
- [34] Fang P. P., Gao C., and Lin J. Bifurcations and dynamics of nonlinear excitations in twisted-bilayer optical lattices. *Chaos, Solitons & Fractals* **195**, 116314 (2025); DOI:10.1016/j.chaos.2025.116314.
- [35] Sundaram S., Burgess C. P., and O’Dell D. H. J., Duality between the quantum inverted harmonic oscillator and inverse square potentials, *New J. Phys.* **26**, 053023 (2024); <https://doi.org/10.1088/1367-2630/ad3a91>.
- [36] Hacker N. and Malomed B. A., Trapping wave fields in an expulsive potential by means of linear coupling, *Phys. Rev. E* **105**, 034213 (2022); DOI: <https://doi.org/10.1103/PhysRevE.105.034213>.
- [37] Reyna A. S. and de Araújo C. B., High-order optical nonlinearities in plasmonic nanocomposites – a review, *Adv. Opt. Phot.* **9**, 720-774 (2017); DOI:10.1364/AOP.9.000720.
- [38] Quiroga-Teixeiro M. and Michinel H., Stable azimuthal stationary state in quintic nonlinear optical media, *J. Opt. Soc. Am. B* **14**, 2004-2009 (1997); <https://doi.org/10.1364/JOSAB.14.002004>.
- [39] Abdullaev F. Kh. and Salerno M., Gap-Townes solitons and localized excitations in low-dimensional Bose-Einstein condensates in optical lattices, *Phys. Rev. A* **72**, 033617 (2005); DOI: <https://doi.org/10.1103/PhysRevA.72.033617>.
- [40] Bakkali-Hassani B., Maury C., Stringari S., Nascimbene S., Dalibard J., and Beugnon J., The cross-over from Townes solitons to droplets in a 2D Bose mixture, *New J. Phys.* **25**, 013007 (2023); <https://doi.org/10.1088/1367-2630/acaee3>.
- [41] Banerjee S., Zhou K., Kant Tiwari S., Tamura, Li R., Kevrekidis P., Mistakidis S. I., Walther V., and Hung C.-L.; Collapse of a Quantum Vortex in an Attractive Two-Dimensional Bose Gas, *Phys. Rev. Lett.* **135**, 073401 (2025); DOI:10.1103/c6wx-zc9x.
- [42] Mansuryan T., Bagley N., Boulesteix R., Arosa Y., Krupa K., Wetzell B., Chaves B. P., Wabnitz S., Couderc V., Aceves A., and Tonello A., Nonlinear flying focus pulses for ultrafast 3D nonlinear microscopy, *Optica* **12**, 1192-1199 (2025); <https://doi.org/10.1364/OPTICA.561661>.
- [43] Boyer V., Godun R. M., Smirne G., Cassetari D., Chandrashekar, C. M., Deb A. B., Laczik Z. J., and Foot C. J., Dynamic manipulation of Bose-Einstein condensates with a spatial light modulator, *Phys. Rev. A* **73**, 031402 (2006); DOI: <https://doi.org/10.1103/PhysRevA.73.031402>.
- [44] Lin Y. J., Perry A. R., Compton, R. L., Spielman, I. B., and Porto J. V., Rapid production of ^{87}Rb Bose-Einstein condensates in a combined magnetic and optical potential, *Phys. Rev. A* **79**, 063631 (2009); DOI: <https://doi.org/10.1103/PhysRevA.79.063631>.
- [45] He C., Shen Y., and Forbes A., Towards higher-dimensional structured light, *Light: Science & Applications* **11**, 205 (2022); <https://doi.org/10.1038/s41377-022-00897-3> www.nature.com/lsa.
- [46] Bai Y., Lv H., Fu X., and Yang Y., Vortex beam: generation and detection of orbital angular momentum [Invited], *Chinese Optics Letters* **20**, 012601 (2022); DOI: 10.3788/COL20220.012601.
- [47] Ahmed H., Kim H., Zhang Y., Intaravanne Y., Jang J., Rho J., Chen S., and Chen X., Optical metasurfaces for generating and manipulating optical vortex beams, *Nanophotonics* **11**, 941-956 (2022); <https://doi.org/10.1515/nanoph-2021-0746> Received November 29, 2021; accepted D
- [48] Lian Y., Qi X., Wang Y., Bai Z., Wang Y., and Lu Z., OAM beam generation in space and its applications: A review, *Optics and Lasers in Engineering* **151**, 106923 (2022); <https://doi.org/10.1016/j.optlaseng.2021.106923>.
- [49] Navon N., Smith R. P., and Hadzibabic Z., Quantum gases in optical boxes, *Nature Physics* **17**, 1334-1341 (2021); DOI:10.1038/s41567-021-01403-z.
- [50] Kim, S. Lee K., Kim J., and Shin Y., Flattening a trapped atomic gas using a programmable optical potential in a feedback loop, *Phys. Rev. A* **110** (2024); DOI: 10.1103/PhysRevA.110.033326.
- [51] Impertro A., Karch S., Wienand J. F., Huh S. J., Schweizer C., Bloch I., and Aidelsburger M., Local Readout and Control of Current and Kinetic Energy Operators in Optical Lattices, *Phys. Rev. Lett.* **133**, 063401 (2024); DOI: <https://doi.org/10.1103/PhysRevLett.133.063401>.

- [52] Bashan G., Eyal A., Tur M., and Arie A., Optically programmable quasi phase matching in four-wave mixing, *Nature Communications* **16**, 6855 (2025); DOI:10.1038/s41467-025-62025-0.
- [53] Olshanii M., Perrin H., and Lorent V., Example of a Quantum Anomaly in the Physics of Ultracold Gases, *Phys. Rev. Lett.* **105**, 095302 (2010); DOI: <https://doi.org/10.1103/PhysRevLett.105.095302>.
- [54] Sakaguchi H. and Malomed B. A., Suppression of the quantum collapse in an anisotropic gas of dipolar bosons, *Phys. Rev. A* **84**, 033616 (2011); DOI: <https://doi.org/10.1103/PhysRevA.84.033616>.
- [55] Tribelsky M. I, Exact solutions to fall of particle to singular potential: classical versus quantum cases, *Proc. R. Soc. A* **479**, 20230366 (2023); <https://doi.org/10.1098/rspa.2023.0366>.
- [56] Zang Y., Gu Y., and Jiang S., Detecting Quantum Anomalies in Open Systems, *Phys. Rev. Lett.* **133**, 106503 (2024); DOI: <https://doi.org/10.1103/PhysRevLett.133.106503>.
- [57] Alexander T. J. and Bergé L., Ground states and vortices of matter-wave condensates and optical guided waves, *Phys. Rev. E* **65**, 026611 (2002); DOI: <https://doi.org/10.1103/PhysRevE.65.026611>.
- [58] Carr L. D. and Clark C. W., Vortices in attractive Bose-Einstein condensates in two dimensions, *Phys. Rev. Lett.* **97**, 010403 (2006); DOI: <https://doi.org/10.1103/PhysRevLett.97.010403>.
- [59] Mihalache D., Mazilu D., Malomed B. A., and Lederer F., Vortex stability in nearly-two-dimensional Bose-Einstein condensates with attraction, *Phys. Rev. A* **73**, 043615 (2006); DOI: <https://doi.org/10.1103/PhysRevA.73.043615>.
- [60] Bogolyubov, N. N., On the theory of superfluidity, *Izv. Akad. Nauk SSSR, Ser. Fiz.* **11**, 77-90 (1947).
- [61] Kapitula T. and Promislow K., *Spectral and Dynamical Stability of Nonlinear Waves*, Springer-Verlag (New York, 2013).
- [62] Sadaka G., Jolivet P., Charalampidis E.G., and Danaila I., Parallel finite-element codes for the Bogoliubov-de Gennes stability analysis of Bose-Einstein condensates, *Comput. Phys. Commun.* **306**, 109378 (2025); <https://doi.org/10.1016/j.cpc.2024.109378>.